 CMES, vol.60, no.1, pp.73-94, 2010

A Topology Optimization of Moderately Thick Plates Based on the Meshless Numerical Method

S.L. Li[1,2], S.Y. Long[1] and G.Y. Li[1]

Abstract: A new implementation of topology optimization for the plate described by the Reissner-Mindlin theory based on the meshless natural neighbour Petrov-Galerkin method (NNPG) is proposed in this work. The objective is to produce the stiffest plate for a given volume by redistributing the material throughout the plate. We try to couple the advantages of the meshless numerical method with the topology optimization of moderately thick plate. The numerical approach presented here is based on the solid isotropic material with penalization (SIMP) formulation of the topology optimization problem. The natural neighbour interpolation shape function is employed to discretize both displacement and bulk density fields. Several examples are provided to illustrate the validity and effectiveness of the proposed method.

Keywords: topology optimization; meshless method; Reissner-Mindlin plate; the natural neighbour interpolation; SIMP

1 Introduction

Topology optimization of the continuum structure is one of the most difficult and challenging areas of the structural optimization [Bendsoe and Sigmund (2003)]. The goal of a typical topology optimization problem is to determine the layout of the most rigid structure capable of supporting a given load, constrained by the amount of material available and restricted spatially to be within a prescribed package space. Ever since Bendsoe and Kikuchi (1988) introduced the topology optimization using a so-called microstructure or homogenization method, many topology optimization methods have been developed including the so-called "power-law approach" or SIMP approach (Solid Isotropic Material with Penalization) [Bendsoe (1989), Zhou and Rozvany (1991), Bendsoe and Sigmund (1999)], the evolution-

[1] State Key Laboratory of Advanced Design and Manufacture for Vehicle Body, Hunan University, Changsha, 410082, China
[2] Corresponding author. E-mail: shunlili66@163.com.

ary approach [Xie and Steven (1993)], the level-set method [Wang et al. (2003)], and the implicit topology description function (ITDF) method [Belytschko et al. (2003)], etc.

Up to now, the prevailing analysis method in the topology optimization is the finite element method (FEM), and most of the numerical methods used in topology optimization literatures are mesh-based methods. However, for these methods, there are some shortcomings such as mesh distortion, frequent remeshing when dealing with large deformation or moving boundary problems, etc. These shortcomings are even more acute when dealing with topology optimization problems. In this kind of problems, it is vital to obtain accurate structural responses. In recent years, considerable efforts have been devoted to develop various meshless methods to avoid the mesh-related difficulties. Many meshless methods have been proposed, such as the smooth particle hydrodynamics (SPH) [Monaghan (1977)], the element-free Galerkin method (EFG) [Belytschko et al. (1994)], the reproducing kernel particle method (RKPM) [Liu et al. (1995)], the meshless local Petrov-Galerkin method (MLPG) [Atluri and Zhu (1998)], the Natural Element Method (NEM) [Braun and Sambridge (1995); Sukumar et al. (1998)] and several others. The meshless local Petrov-Galerkin method (MLPG) which based on local weak formulation proposed a new integration method in a local domain and permits trial and test functions from different spaces. Remarkable successes of the MLPG and their variation have been reported in high-speed impact, penetration and perforation Problems [Han et al. (2006)], dynamic fracture problems [Gao et al. (2006)], elastic transient analysis [Sellountos et al. (2009)], etc. Recently, the natural neighbour Petrov-Galerkin method (NNPG) was proposed by Wang et al (2005), which intends to combine the advantage of easy imposition of essential boundary conditions of the NEM with some prominent features of the MLPG.

Plate structures are widely used in many engineering structures. It is well known that the classical thin plate theory of Kirchhoff gives rise to certain non-physical simplifications from the omission of the shear deformations and rotary inertia, which are growing significantly for increasing thickness of the plate. The effects of shear deformation and rotary inertia are taken into account in the Reissner–Mindlin plate bending theory [Reissner (1945), Mindlin (1951)]. In recent years, the analysis of Reissner–Mindlin plates by meshless methods has been object of attention and studied extensively. The elastic analysis of Reissner-Mindlin plates was considered in Donning and Liu (1998) using the EFG and in Garcia et al. (2000) resorting to the hp-clouds method. The Elasto-plastic analysis of Reissner–Mindlin plates by the EFG has been reported in Belinha and Dinis (2006). Geometrically nonlinear analysis of Reissner-Mindlin plate by the meshless collocation method was given by Wen and Hon (2007). Dynamic bending problems and viscoelastic

analysis of Reissner-Mindlin plate were studied by Sladek et al (2007, 2008a) resorting to the MLPG. Sladek et al (2008b) also applied the MLPG to the thermal analysis of Reissner-Mindlin shallow shells with FGM properties. The problem of finding optimum topologies for plate structures has been treated extensively in the literature. The use of topology design in general and the homogenization approach in particular for Mindlin plates and shells is discussed in Soto and Diaz (1993), Diaz et al (1995), Lipton and Diaz (1997). Topology optimization of plates with prestress was given by Pedersen (2001). Maximizing the band gap size for bending waves in a Mindlin plate is the theme of Halkjær et al (2006). Topological material layout in plates for vibration suppression and wave propagation control was considered in Larsen et al (2009).

In the present paper, a new implementation of the topology optimization for Reissner-Mindlin plate using the meshless natural neighbour Petrov-Galerkin method (NNPG) is proposed. In most papers that deal with the optimization of plate the problem is formulated as a case of reinforcement optimization, and the topology optimization problem is formulated using the homogenization method. In this case it is the reinforcement which is topology optimized and not the basic structure. In the present paper, based on a meshless NNPG model of the plate, the SIMP formulation of the topology optimization problem and the optimality criteria method for iterative optimization will be used. In the NNPG, the trial functions on a local domain are constructed using the natural neighbour interpolation and shape functions of the three-node triangular element in FEM are taken as test functions. The natural neighbour interpolation shape function which has Kronecker Delta function property is employed to discretize both displacement and bulk density fields. The checkerboard layout is one of the frequently encountered numerical instabilities in the topology optimization. To ensure existence of solutions, the SIMP approach must be combined with a perimeter constraint, a gradient constraint or with filtering techniques [Sigmund and Petersson (1998)]. However, by virtue of the continuous density fields employed in this work (The natural neighbour interpolants are smooth everywhere, except at the nodes where they are C^0), the proposed method effectively eliminates checkerboard patterns of the material distribution without using any extra filtering techniques.

The outline of this paper is as follows. In Section 2, a brief review of the natural neighbour interpolation is presented. In Section 3, we briefly describe the NNPG method for the Reissner-Mindlin plate bending problems. The formulations of the topology optimization for plates based on the meshless NNPG method are given in Section 4. In Section 5, several numerical examples of topology optimization problems are presented to demonstrate the validity and feasibility of the proposed method. The paper ends with some conclusions that are presented in Section 6.

2 Natural neighbour interpolation

The natural neighbour interpolation is based on the well-known Voronoi diagram and Delaunay tessellation. Consider a set of distinct nodes $N = \{n_1, n_2, \cdots, n_M\}$ in R^2. The Voronoi diagram (or 1st-order Voronoi diagram) of the set N is a subdivision of the plane into regions T_i, where each region T_i is associated with a node n_i, such that any point in T_i is closer to n_i (nearest neighbour) than to any other node $n_j \in N\,(j \neq i)$, in mathematical terms:

$$T_i = \left\{ \mathbf{x} \in R^2 : d(\mathbf{x}, \mathbf{x}_i) < d(\mathbf{x}, \mathbf{x}_j) \forall j \neq i \right\} \tag{1}$$

where $d(\mathbf{x}, \mathbf{x}_i)$ is the distance between $\mathbf{x}$ and $\mathbf{x}_i$. The Voronoi cell T_i is the intersection of finitely many open half-spaces, being delimited by the perpendicular bisectors of the lines which connect the node n_i with its natural neighbours. The Delaunay triangulation, which is the dual of the Voronoi diagram, is constructed by connecting the nodes whose Voronoi cells have common boundaries. The important property of Delaunay triangles is the empty circumcircle criterion—if $\mathrm{DT}(n_j, n_k, n_l)$ is any Delaunay triangle of the nodal set N, then the circumcircle of DT contains no other nodes of N. This criterion is used to find the natural neighbours of a point $\mathbf{x}$ (like integration points). If the point $\mathbf{x}$ lies within the circumcircle of a triangle $\mathrm{DT}(n_j, n_k, n_l)$, then n_j, n_k and n_l are its natural neighbours. The Voronoi diagram and the Delaunay triangulation of a set of nodes are shown in Figure 1.

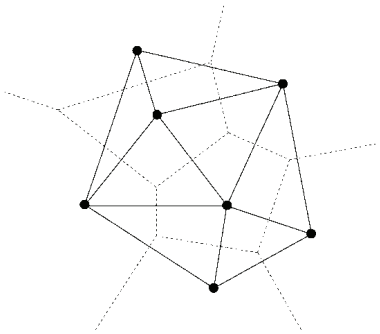

Figure 1: Voronoi diagram, Delaunay triangulation of a set of nodes

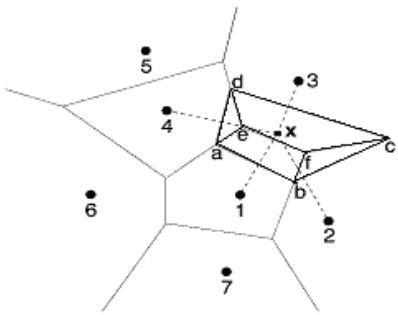

Figure 2: Construction of natural neighbour coordinates

In order to quantify the neighbour relation for any point $\mathbf{x}$ introduced into the tessellation, the second-order Voronoi cell of point $\mathbf{x}$ is constructed as shown in Figure 2. The natural neighbour shape function of $\mathbf{x}$ with respect to a natural neighbour i

is defined as the ratio of the area of overlap of their Voronoi cells to the total area of the Voronoi cell of $\mathbf{x}$:

$$\Phi_i(\mathbf{x}) = A_i(\mathbf{x}) / A(\mathbf{x}) \tag{2}$$

where i ranges from 1 to n (the number of the natural neighbours of point $\mathbf{x}$), and $A(\mathbf{x}) = \sum_{j=1}^{n} A_j(\mathbf{x})$. The four regions shown in Figure 2 are the second-order cells, while their union (closed polygon *abcd*) is the first-order Voronoi cell. Referring to Figure 2, the shape function $\Phi_1(\mathbf{x})$ is given by

$$\Phi_1(\mathbf{x}) = A_{abfe} / A_{abcd} \tag{3}$$

The derivatives of the shape functions are obtained by differentiating equation (2):

$$\Phi_{i,j}(\mathbf{x}) = \frac{A_{i,j}(\mathbf{x}) - \Phi_i(\mathbf{x}) A_{,j}(\mathbf{x})}{A(\mathbf{x})} \quad (j = 1,2) \tag{4}$$

The displacement approximations $\mathbf{u}^h(\mathbf{x})$ of point $\mathbf{x}$ can be written as

$$\mathbf{u}^h(\mathbf{x}) = \sum_{i=1}^{n} \Phi_i(\mathbf{x}) \mathbf{u}_i \tag{5}$$

where $\mathbf{u}_i$ $(i = 1, \cdots, n)$ are the vectors of nodal displacements at the n natural neighbours, and $\Phi_i(\mathbf{x})$ are the shape functions associated with each node.

By definition of the shape function given in equation (2), the following remarkable properties that are important to construct the approximation functional spaces is self-evident [Sukumar et al. (1998)]:

$$0 \leq \Phi_i(\mathbf{x}) \leq 1 \tag{6}$$

$$\Phi_i(\mathbf{x}_j) = \delta_{ij} \tag{7}$$

$$\sum_{i=1}^{n} \Phi_i(\mathbf{x}) = 1 \tag{8}$$

$$\mathbf{x} = \sum_{i=1}^{n} \Phi_i(\mathbf{x}) \mathbf{x}_i \tag{9}$$

Equation (7) implies that the NEM interpolant passed through the nodal values, and the essential boundary conditions can be imposed directly. Equations (8) and (9) defines a partition of unity and linear completeness, which imply that the shape functions can reproduce the rigid body displacement and the constant strain. The more detailed discussion of the NEM interpolation can be found in Sukumar et al. (1998).

3 Governing equations for the Reissner-Mindlin plate theory and their local weak form

Consider an elastic plate of constant thickness h with a domain Ω, the $x_1 - x_2$ plane is assumed to coincide with the mean surface of the plate. The governing equations of the Reissner-Mindlin plate for bending problem can be expressed as

$$M_{ij,j} - Q_i = 0 \quad i,j = 1,2; \text{ in } \Omega \tag{10}$$

$$Q_{i,i} + q = 0 \quad i = 1,2; \text{ in } \Omega \tag{11}$$

Where M_{ij} denote the bending and torsional moments, Q_i are the shear forces, and q is the transverse load on the middle plane in unit area. M_{ij} and Q_i are expressed in terms of the rotations and the lateral displacement as

$$M_{ij} = \frac{1-\nu}{2} D \left(\theta_{i,j} + \theta_{j,i} + \frac{2\nu}{1-\nu} \theta_{\gamma,\gamma} \delta_{ij} \right) \tag{12}$$

$$Q_i = \frac{D(1-\nu)}{2} \lambda^2 (\theta_i + w_{,i}) \tag{13}$$

Where θ_i denotes the rotation in the x_i- direction, w represents the out-of-plane deflection, $D = Eh^3 / \left[12\left(1-\nu^2\right)\right]$ denotes the plate flexural stiffness, with E being Young's modulus, ν being Poisson's ratio, and $\lambda^2 = 10/h^2$ is the shear correction factor of the Reissner theory. The shear correction factor κ^2 of the Mindlin theory is usually taken as $5/6$ in order for the two theories to coincide provided that $\lambda^2 = 12\kappa^2/h^2$.

As the natural neighbour shape functions have the Kronecker delta function property, neither Lagrange multiplier nor penalty parameter is needed to impose the essential boundary condition. In sub-domain Ω_s which is a small region taken for each node, the generalized local weak form of the governing equations (10) and (11) can be written as

$$\int_{\Omega_s} W_I (M_{ij,j} - Q_i) d\Omega = 0 \tag{14}$$

$$\int_{\Omega_s} W_I (Q_{i,i} + q) d\Omega = 0 \tag{15}$$

where W_I is the test function. Using Gaussian divergence theorem, Equation (14) can be written as

$$\int_{\Gamma_s} W_I M_{ij} n_j d\Gamma - \int_{\Omega_s} W_{I,j} M_{ij} d\Omega - \int_{\Omega_s} W_I Q_i d\Omega = 0 \tag{16}$$

that is

$$\int_{\Omega_s} \begin{bmatrix} W_{I,x} & 0 & W_{I,y} \\ 0 & W_{I,y} & W_{I,x} \end{bmatrix} \begin{Bmatrix} M_x \\ M_y \\ M_{xy} \end{Bmatrix} d\Omega - \int_{\Gamma_s} W_I \begin{bmatrix} n_x & 0 & n_y \\ 0 & n_y & n_x \end{bmatrix} \begin{Bmatrix} M_x \\ M_y \\ M_{xy} \end{Bmatrix} d\Gamma + \int_{\Omega_s} W_I \begin{Bmatrix} Q_x \\ Q_y \end{Bmatrix} d\Omega = 0 \quad (17)$$

Analogously, equation (15) can be written as

$$\int_{\Gamma_s} W_I Q_i n_i d\Gamma - \int_{\Omega_s} W_{I,i} Q_i d\Omega + \int_{\Omega_s} W_I q d\Omega = 0 \quad (18)$$

that is

$$\int_{\Omega_s} \begin{bmatrix} W_{I,x} & W_{I,y} \end{bmatrix} \begin{Bmatrix} Q_x \\ Q_y \end{Bmatrix} d\Omega - \int_{\Gamma_s} W_I \begin{bmatrix} n_x & n_y \end{bmatrix} \begin{Bmatrix} Q_x \\ Q_y \end{Bmatrix} d\Gamma - \int_{\Omega_s} W_I q d\Omega = 0 \quad (19)$$

Combining equations (17) and (19) gives

$$\int_{\Omega_s} \begin{bmatrix} W_{I,x} & 0 & W_{I,y} & W_I & 0 \\ 0 & W_{I,y} & W_{I,x} & 0 & W_I \\ 0 & 0 & 0 & W_{I,x} & W_{I,y} \end{bmatrix} \begin{Bmatrix} M_x \\ M_y \\ M_{xy} \\ Q_x \\ Q_y \end{Bmatrix} d\Omega - \int_{\Gamma_s} W_I \begin{bmatrix} n_x & 0 & n_y & 0 & 0 \\ 0 & n_y & n_x & 0 & 0 \\ 0 & 0 & 0 & n_x & n_y \end{bmatrix} \begin{Bmatrix} M_x \\ M_y \\ M_{xy} \\ Q_x \\ Q_y \end{Bmatrix} d\Gamma - \int_{\Omega_s} W_I \begin{Bmatrix} 0 \\ 0 \\ q \end{Bmatrix} d\Omega = 0 \quad (20)$$

succinctly as

$$\int_{\Omega_s} \mathbf{L} W_I \boldsymbol{\sigma} d\Omega - \int_{\Gamma_s} W_I \bar{\mathbf{N}} \boldsymbol{\sigma} d\Gamma - \int_{\Omega_s} W_I \mathbf{b} d\Omega = 0 \quad (21)$$

Where

$$\mathbf{L} = \begin{bmatrix} \frac{\partial}{\partial x} & 0 & \frac{\partial}{\partial y} & 1 & 0 \\ 0 & \frac{\partial}{\partial y} & \frac{\partial}{\partial x} & 0 & 1 \\ 0 & 0 & 0 & \frac{\partial}{\partial x} & \frac{\partial}{\partial y} \end{bmatrix} \quad (22)$$

$$\bar{\mathbf{N}} = \begin{bmatrix} n_x & 0 & n_y & 0 & 0 \\ 0 & n_y & n_x & 0 & 0 \\ 0 & 0 & 0 & n_x & n_y \end{bmatrix} \tag{23}$$

$$\boldsymbol{\sigma} = \begin{bmatrix} M_x & M_y & M_{xy} & Q_x & Q_y \end{bmatrix}^T \tag{24}$$

$$\mathbf{b} = \begin{bmatrix} 0 & 0 & q \end{bmatrix}^T \tag{25}$$

Where the boundary Γ_s for the sub-domain Ω_s usually consists of three parts: the internal boundary Γ_{si}, which does not intersect with the global boundary, the boundary Γ_{su} and Γ_{st}, over which the essential and natural boundary conditions are prescribed. Noting that $n_j \sigma_{ij} = \bar{t}_i$ holds on the Γ_{st}, equation (21) becomes

$$\int_{\Omega_s} \mathbf{L} W_I \boldsymbol{\sigma} d\Omega - \int_{\Gamma_{su}} W_I \bar{\mathbf{N}} \boldsymbol{\sigma} d\Gamma - \int_{\Gamma_{si}} W_I \bar{\mathbf{N}} \boldsymbol{\sigma} d\Gamma = \int_{\Omega_s} W_I \mathbf{b} d\Omega + \int_{\Gamma_{st}} W_I \bar{\mathbf{t}} d\Gamma \tag{26}$$

For a sub-domain located entirely within the global domain, there is no intersection with the global boundary, in such a case, the integrals over Γ_{su} and Γ_{st} vanish. To simplify the above equation, the test function W_I can be deliberately selected such that the support of test function W_I is coincident with sub-domain Ω_s. This can be easily accomplished by selecting the three-node triangular FEM shape function N_I as test function. As a result, the integral over Γ_{si} vanishes due to the zero value of the test function, and the continuous form of the NNPG formulation for Reissner-Mindlin plate theory is obtained

$$\int_{\Omega_s} \mathbf{L} N_I \boldsymbol{\sigma} d\Omega - \int_{\Gamma_{su}} N_I \bar{\mathbf{N}} \boldsymbol{\sigma} d\Gamma = \int_{\Omega_s} N_I \mathbf{b} d\Omega + \int_{\Gamma_{st}} N_I \bar{\mathbf{t}} d\Gamma \tag{27}$$

For the numerical implementation, the discrete form of equation (27) is used, which is obtained by substituting the approximation of the displacement (5) into equation (27).

$$\int_{\Omega_s} \mathbf{V}_{dI} \mathbf{D} \mathbf{B} \mathbf{u} d\Omega - \int_{\Gamma_{su}} \mathbf{V}_I \bar{\mathbf{N}} \mathbf{D} \mathbf{B} \mathbf{u} d\Gamma = \int_{\Omega_s} \mathbf{V}_I \mathbf{b} d\Omega + \int_{\Gamma_{st}} \mathbf{V}_I \bar{\mathbf{t}} d\Gamma \tag{28}$$

Where $\mathbf{u} = \begin{bmatrix} (\theta_x)_1 & (\theta_y)_1 & w_1 & \cdots & (\theta_x)_n & (\theta_y)_n & w_n \end{bmatrix}^T$ is the vector of nodal displacements. For simplicity, the matrix forms of the discrete equations can be written as

$$(\mathbf{K}_I)_{3\times 3n} \mathbf{u}_{3n\times 1} = (\mathbf{F}_I)_{3\times 1} \tag{29}$$

where $\mathbf{K}_I$ and $\mathbf{F}_I$ are the nodal stiffness matrix and nodal force vector of the node I, respectively.

$$\mathbf{K}_I = \int_{\Omega_s} \mathbf{V}_{dI} \mathbf{D} \mathbf{B} d\Omega - \int_{\Gamma_{su}} \mathbf{V}_I \bar{\mathbf{N}} \mathbf{D} \mathbf{B} d\Gamma \tag{30}$$

$$\mathbf{F}_I = \int_{\Omega_s} \mathbf{V}_I \mathbf{b} d\Omega + \int_{\Gamma_{st}} \mathbf{V}_I \bar{\mathbf{t}} d\Gamma \tag{31}$$

In above equations, $\mathbf{B}$ is the strain matrix, and $\mathbf{D}$ is the constant material matrix. $\mathbf{V}_I$ and $\mathbf{V}_{dI}$ are the matrices of test function and their derivative, respectively. These matrices are defined as follows:

$$\mathbf{B} = \begin{bmatrix} \Phi_{1,x} & 0 & 0 & \cdots & \Phi_{n,x} & 0 & 0 \\ 0 & \Phi_{1,y} & 0 & \cdots & 0 & \Phi_{n,y} & 0 \\ \Phi_{1,y} & \Phi_{1,x} & 0 & \cdots & \Phi_{n,y} & \Phi_{n,x} & 0 \\ \Phi_1 & 0 & \Phi_{1,x} & \cdots & \Phi_n & 0 & \Phi_{n,x} \\ 0 & \Phi_1 & \Phi_{1,y} & \cdots & 0 & \Phi_n & \Phi_{n,y} \end{bmatrix} \tag{32}$$

$$\mathbf{D} = \begin{bmatrix} D & \nu D & 0 & 0 & 0 \\ \nu D & D & 0 & 0 & 0 \\ 0 & 0 & \frac{(1-\nu)D}{2} & 0 & 0 \\ 0 & 0 & 0 & \frac{(1-\nu)D}{2}\lambda^2 & 0 \\ 0 & 0 & 0 & 0 & \frac{(1-\nu)D}{2}\lambda^2 \end{bmatrix} \tag{33}$$

$$\mathbf{V}_I = \begin{bmatrix} N_I & 0 & 0 \\ 0 & N_I & 0 \\ 0 & 0 & N_I \end{bmatrix} \tag{34}$$

$$\mathbf{V}_{dI} = \begin{bmatrix} N_{I,x} & 0 & N_{I,y} & N_I & 0 \\ 0 & N_{I,y} & N_{I,x} & 0 & N_I \\ 0 & 0 & 0 & N_{I,x} & N_{I,y} \end{bmatrix} \tag{35}$$

It must be noted that equation (29) represents three linear equations for the sub-domain of the Ith field node, therefore a total of $3N$ equations can be obtained for all N field nodes. The final discrete system equations can be written as follows:

$$\mathbf{K}_{(3N\times 3N)}\mathbf{U}_{(3N\times 1)} = \mathbf{F}_{(3N\times 1)} \tag{36}$$

To numerically implement the NNPG, the sub-domains need to be defined. In NNPG, a set of distinct nodes are placed in the global domain and on its boundary, and the domain is subdivided by Delaunay tessellations. Each node in the global domain and on the boundary, e.g. node I, is associated with a local sub-domain Ω_s, which is constructed by collecting all the surrounding Delaunay triangles with node I being their common vertices. In each sub-domain, the three-node triangular FEM shape function N_I is used as the test function. In the implementation, the domain integrals over Ω_s can be evaluated by the summation of the integrals over included Delaunay triangles with Gaussian quadrature scheme. In the present work, three Gaussian points are used for domain integrals in each triangular region and two Gaussian points are used for boundary integrals.

4 Formulation of the topology optimization design based on NNPG

In the topology design of a structure we are interested in the determination of the optimal placement of a given isotropic material in space, i.e., we should determine which points of space should be material points and which points should remain void (no material) [Bendsoe and Sigmund (2003)]. The most commonly used approach to solve this discrete valued design problem (0-1 problem) is to replace the integer variables with continuous variables and then introduce some form of penalty that steers the solution to discrete 0-1 values. In present paper, the very popular and extremely efficient SIMP approach [Bendsoe (1989)] is used.

$$\begin{array}{l} E_{ijkl}(\mathbf{x}) = \rho(\mathbf{x})^P E^0_{ijkl} \quad P > 1 \\ \int_\Omega \rho(\mathbf{x})\, d\Omega \le V;\ 0 \le \rho(\mathbf{x}) \le 1 \quad \mathbf{x} \in \Omega \end{array} \tag{37}$$

Here $\rho(\mathbf{x})$ which resembles a density of material is the design variable, P is the penalty factor that penalizes the intermediate values of this artificial density function, E^0_{ijkl} represents the material properties of a given isotropic material, and V is the amount of material at our disposal. In the SIMP, $P > 1$ is chosen so that intermediate densities are unfavourable in the sense that the stiffness obtained is small compared to the cost (volume) of the material.

The natural neighbour interpolation shape function is employed to discretize the bulk density fields.

$$\rho(\mathbf{x}) = \sum_{i=1}^{np} \Phi_i(\mathbf{x})\, \rho_i \tag{38}$$

Where ρ_i is the nodal relative density of the ith node, $\Phi_i(\mathbf{x})$ is the same natural neighbour interpolation shape function which is employed to discretize the displacement field in the structural response analysis, and np is the number of natural neighbours of $\mathbf{x}$.

A topology optimization for plate bending problem based on the SIMP approach, where the objective is to minimize compliance, can be formulated in the NNPG method context as follows:

$$\begin{array}{rl} & \text{find } \rho(\mathbf{x}),\ \mathbf{x} \in \Omega \\ & \text{min: } c = \mathbf{F}^T \mathbf{U} \\ \text{subject to:} & \mathbf{KU} = \mathbf{F} \\ & : E_{ijkl}(\mathbf{x}) = \rho(\mathbf{x})^P E^0_{ijkl} \\ & : V = \int_\Omega \rho(\mathbf{x})\, d\Omega = fV_0;\ 0 < \rho_{\min} \le \rho_i \le 1 \end{array} \tag{39}$$

where $\mathbf{U}$ and $\mathbf{F}$ are the global displacement and force vectors, respectively, $\mathbf{K}$ is the global stiffness matrix, V and V_0 are the material volume and design domain, respectively, f is the prescribed volume fraction, and $\rho_{\min}$ is a lower bound on the density which introduced to prevent any possible singularity, $\rho_{\min} = 0.001$ is used in this paper.

The optimization problem (39) could be solved using several different approaches such as Optimality Criteria (OC) method [Bendsoe and Kikuchi (1988), Zhou and Rozvany (1991)], Sequential Linear Programming (SLP) method [Fujii and Kikuchi (2000)] or Method of Moving Asymptotes (MMA) [Svanberg (1987)] and others. Since OC method is easy to understand and implement, and is an effective method for solving large scale problems which comes from the fact that each design variable is updated independently of the update of the other design variables; OC method is used in this work. Following Sigmund (2001), a heuristic updating scheme for the design variables can be formulated as

$$\rho_i^{\text{new}} = \begin{cases} \max(\rho_{\min}, \rho_i - m) & \text{if } \rho_i B_i^{\eta} \leq \max(\rho_{\min}, \rho_i - m) \\ \rho_i B_i^{\eta} & \text{if } \max(\rho_{\min}, \rho_i - m) < \rho_i B_i^{\eta} < \min(1, \rho_i + m) \\ \min(1, \rho_i + m) & \text{if } \min(1, \rho_i + m) \leq \rho_i B_i^{\eta} \end{cases} \tag{40}$$

where m is a move limit and η is a tuning parameter, which control the changes that happen at each iteration step and they can be made adjustable for efficiency of the method; and B_i is found from the optimality condition as

$$B_i = -\frac{\partial c}{\partial \rho_i} \left(\lambda \frac{\partial V}{\partial \rho_i} \right)^{-1} \tag{41}$$

where λ is a Lagrange multiplier which should be adjusted in an inner iteration loop in order to satisfy the active volume constraint and can be found by a bisection method.

In order to complement the presentation of the optimality criteria method, we will here work with the sensitivity analysis of the minimum compliance problem formulated in equation (39). Referring to the sensitivity analysis in the FEM form, the adjoint method is used to obtain the sensitivity of the objective function. We rewrite the objective function by adding the zero function:

$$c = \mathbf{F}^T \mathbf{U} - \tilde{\mathbf{U}}^T (\mathbf{K}\mathbf{U} - \mathbf{F}) \tag{42}$$

where $\tilde{\mathbf{U}}$ is any arbitrary, but fixed real vector. By the differentiation of above equation with respect to the design variable ρ_i, after rearrangement of terms, we

obtain as

$$\frac{\partial c}{\partial \rho_i} = \left(\mathbf{F}^T - \tilde{\mathbf{U}}^T \mathbf{K}\right) \frac{\partial \mathbf{U}}{\partial \rho_i} - \tilde{\mathbf{U}}^T \frac{\partial \mathbf{K}}{\partial \rho_i} \mathbf{U} \tag{43}$$

This can be written as

$$\frac{\partial c}{\partial \rho_i} = -\tilde{\mathbf{U}}^T \frac{\partial \mathbf{K}}{\partial \rho_i} \mathbf{U} \tag{44}$$

when $\tilde{\mathbf{U}}$ satisfies the adjoint equation:

$$\mathbf{F}^T - \tilde{\mathbf{U}}^T \mathbf{K} = 0 \tag{45}$$

Since the stiffness matrix $\mathbf{K}$ in the NNPG is asymmetric, $\tilde{\mathbf{U}}$ is normally not equal to $\mathbf{U}$. In contrast to the approach in FEM form, the adjoint equation requires additional computations in this work. In this way, the derivatives of the displacement are no need to calculate explicitly. The derivative of the volume constraint with respect to the design variable is obtained as follows

$$\frac{\partial V}{\partial \rho_i} = \int_\Omega \Phi_i d\Omega \tag{46}$$

5 Numerical examples

In this section, several topology optimization problems of plates are chosen as examples to demonstrate the validity and feasibility of the proposed method. In all these examples, the elastic material properties are chosen as Young's modulus $E = 2 \times 10^{11}$Pa and Poisson's ratio $\nu = 0.3$. A move limit $m = 0.2$ and a tuning parameter $\eta = 0.5$ are chosen in this work.

To test the convergence and the accuracy of the present method, a uniformly loaded clamped square plate with side length $a = 1.0$m and plate thickness $h = 0.2$m is considered. For convergence study, the deflection norms is defined as below

$$\| w \| = \left(\int_\Omega w^2 d\Omega \right)^{1/2} \tag{47}$$

The relative error of the deflection is defined as

$$r = \frac{\| w^{\mathrm{n}} - w^{\mathrm{e}} \|}{\| w^{\mathrm{e}} \|} \tag{48}$$

where the superscripts n and e denote the numerical solutions and exact solutions, respectively. As "exact" solutions, the FEM results have been used, where a very

fine mesh discretization with 1600 quadrilateral eight-node shell elements has been applied. The relative error of the bending moments is defined similarly. To study the convergence of the method, three regular node distributions with 21 by 21, 33 by 33, 41 by 41 nodes, respectively, are used for the discretization of the domain. The density of nodes can be characterized by the distance of two neighbouring nodes s. The relative errors and the convergence rates for central deflection and bending moment are shown in Figure 3. The convergence rates for both quantities are pretty high. The relative error of the central deflection is a little lower than for bending moment. For the finest node distribution with 41 by 41 nodes the relative error for the central deflection is 0.148% and for the bending moment 0.297%, which conforms that the present numerical method for Reissner-Mindlin plate is highly accurate.

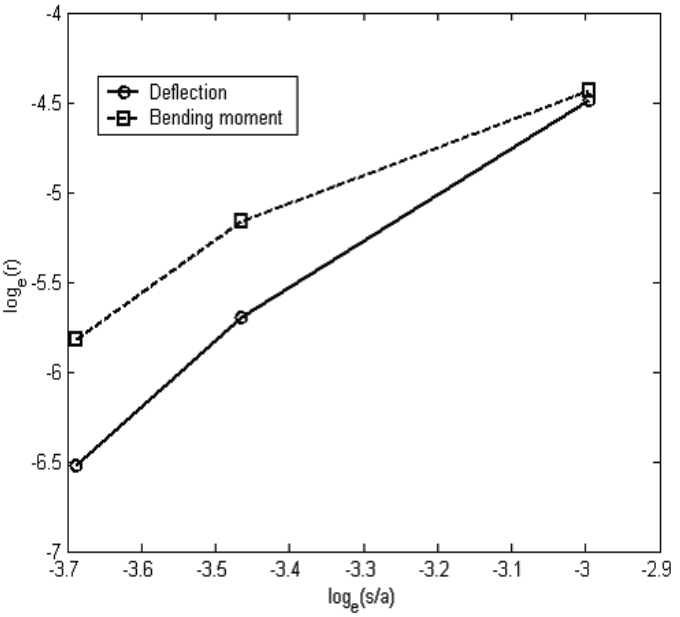

Figure 3: Relative errors and convergence rates for the central deflection and the bending moment of a clamped plate.

In the second example, a square clamped plate of constant thickness h with side length $a = 1.5$m and a concentrated force $F = 1.0 \times 10^6$N applied at the central of the plate is discussed. A regular node distribution with 31 by 31 nodes is used for the discretization of the problem domain, and the penalty factor $P = 3.0$ is used. The topology optimized results obtained by the present method are shown in Figure

4. As we can see from Figure 4, by our optimizing, the mid areas of four clamped edges and central area of the plate, where the bending moments are the largest and second large areas respectively, are strongly reinforced by redistributing the given material in space.

In the third example, a square cantilever plate subjected to two downwards forces at the free end is optimized (see load case 1 in Figure 5). The following geometrical parameters are used in our optimization: the side length of the plate $a = 1.5$m, and the thickness $h = 0.1$m. Again, a regular node distribution with 31 by 31 nodes is used for the discretization of the problem domain, and the penalty factor $P = 3.0$ is used. Figure 6 shows the intermediate steps during the optimization process for square Reissner-Mindlin cantilever plate loaded with two downward oriented forces, the final topology optimized design is shown in Figure 6(e).

It should be noticed that all the analysis are carried out in a meshless manner not a standard lattice mesh, the optimized designs are represented by the relative density distribution of field nodes (the relative density of each field node is between 0 and 1). The same cantilever plate described in the third example subjected to one downwards force and one upwards force at the free end (see load case 2 in Figure 5) is also considered. The topology optimized design of the square cantilever plate obtained by the present method with 31 by 31 nodal discretization is shown in Figure 7 (Only the field nodes whose relative densities are bigger than 0.8 are shown).

In the last example, the same square plate described in the second example but with four edges simply supported is investigated. In our numerical tests, the hardly penalization of the intermediate densities is inadvisable at the beginning of the optimization, the penalty factor $P = 2.2$ is chosen in this example. Resulting topology for compliance minimization of the square Reissner-Mindlin plates with four edges simply supported is shown in Figure 8.

For convergence studies, the step-variations of compliance in the optimization process both for the clamped plate and simply supported plate are given in Figure 9. Apparently, the topology optimized design for clamped plate is much stiffer than for simply supported plate by the same material constraints, the compliance of topology design for simply support plate is about 2.67 times by that for clamped plate. The convergence speed of the topology optimization for simply supported plate is little slower than clamped plate by virtue of choosing the smaller penalty factor.

6 Conclusions

In this paper, a new implementation of the topology optimization for the Reissner-Mindlin plate using the meshless natural neighbour Petrov-Galerkin method (NNPG)

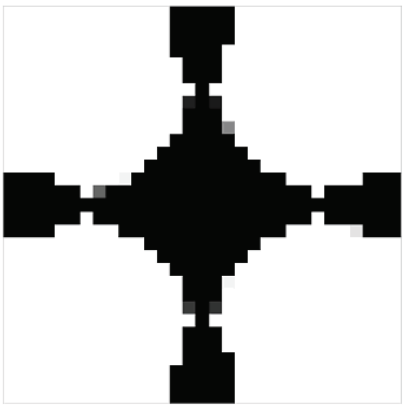

(a): h=0.1m, f=0.25

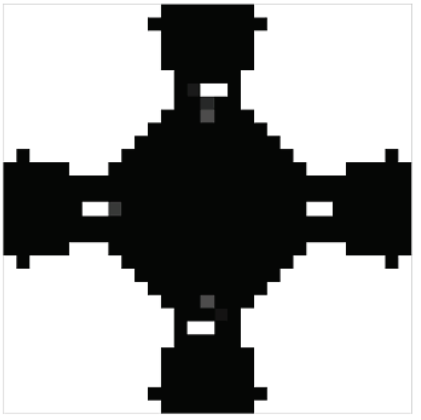

(c): h=0.1m, f=0.4

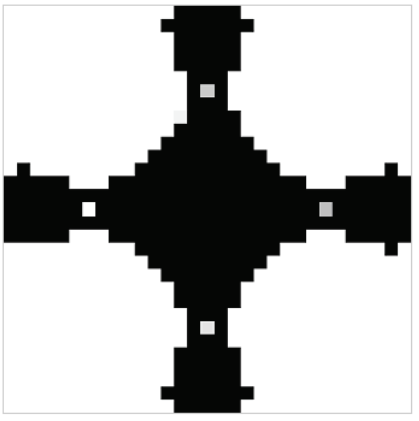

(b): h=0.1m, f=0.3

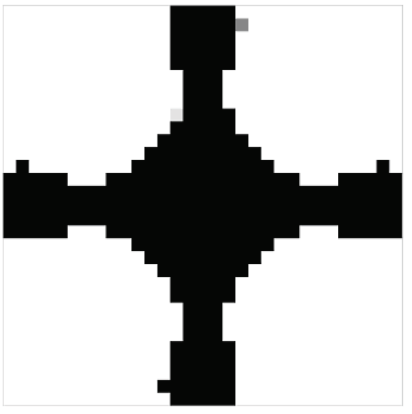

(d): h=0.2m, f=0.3

Figure 4: Resulting topologies for compliance minimization of square Reissner-Mindlin plates with four edges clamped. The material volumes are restricted to 0.25, 0.3 and 0.4, respectively.

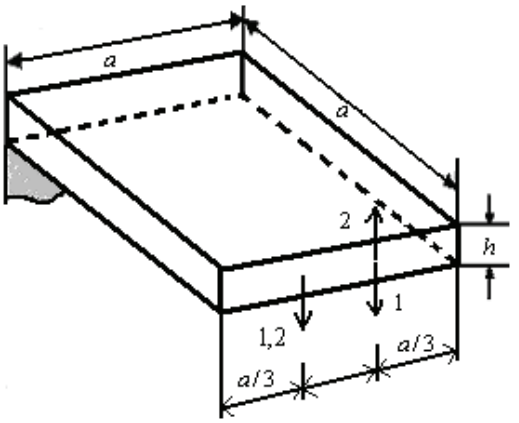

Figure 5: Design problem with loads.

has been described.

In the NNPG, the trial functions on a local domain are constructed based on the natural neighbour interpolation and shape functions of the three-node triangular element in FEM are taken as test functions, which reduces the order of integrands involved in domain integrals and no stiffness matrix assembly is required. The natural neighbour interpolation shape functions have the Kronecker Delta function property, which facilitates imposition of essential boundary conditions.

The structural response analysis, the sensitivity analysis as well as the bulk density field are all approximated by the natural neighbour interpolation shape functions in a meshless manner. In the optimization process, the mesh distortion of mesh-based methods can be completely eliminated and without requiring remeshing.

Several topology optimization problems for plate are solved successfully by the proposed method. Our numerical examples demonstrate that the proposed method is valid and capable to deal with topology optimization problems. By virtue of the continuous density fields employed in this work, the checkerboard pattern of material distribution is prevented in our numerical examples even if without using any extra filtering techniques.

Acknowledgement: This work is supported by National 973 Scientific and Technological Innovation Project (2010CB3228005), Natural Science Foundation of China (No. 10672055) and the Science Fund of State Key Laboratory of Advanced Design and Manufacturing for Vehicle Body (No. 60870003).

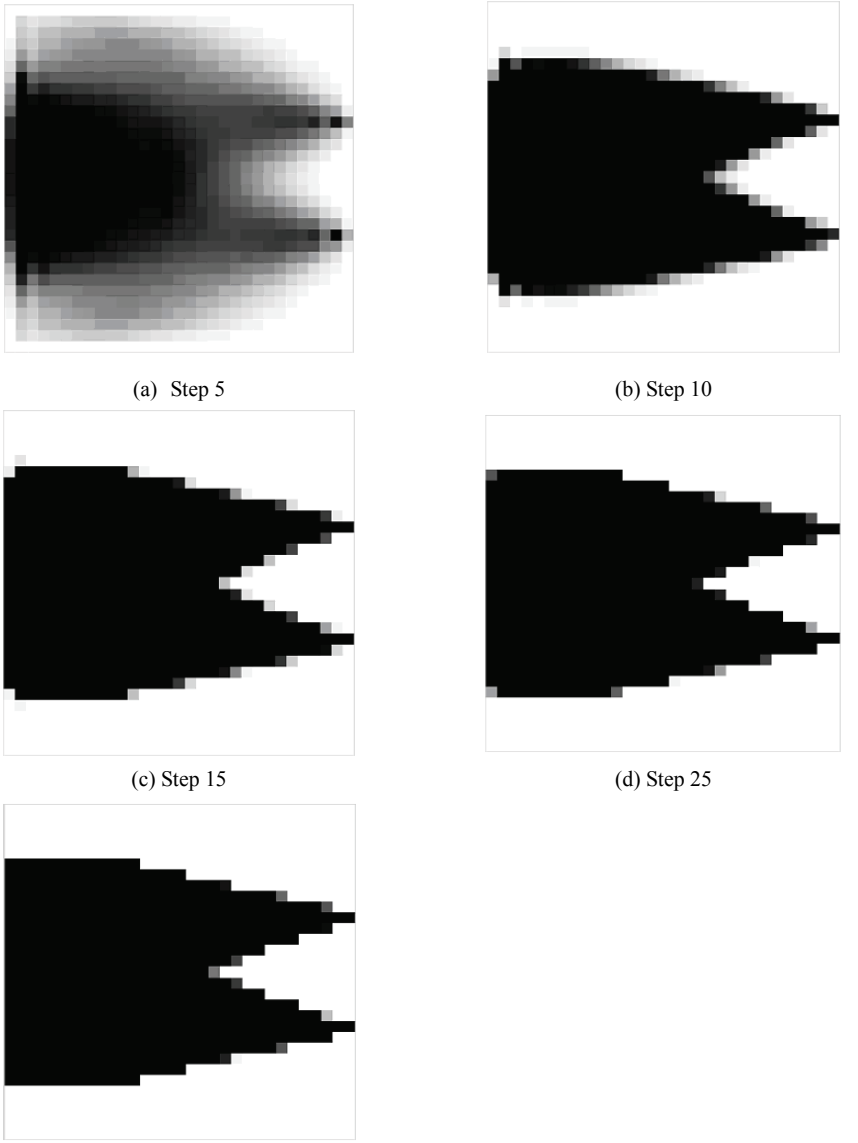

(a) Step 5

(b) Step 10

(c) Step 15

(d) Step 25

(e) Final topology optimized design

Figure 6: Optimization process for a square Reissner-Mindlin cantilever plate loaded with two downward oriented forces: (a) step 5; (b) step 10; (c) step15; (d) step 25; (e) final design. The material volume fraction is 50%.

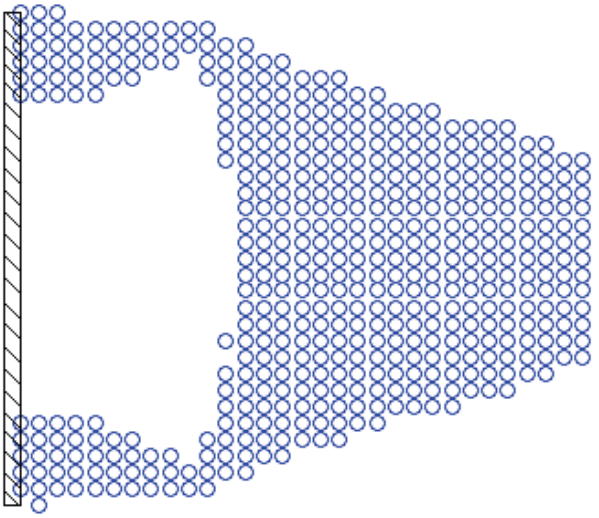

Figure 7: Resulting topology for compliance minimization of square Reissner-Mindlin cantilever plate loaded with one force downwards and one upwards. The material volume fraction is 50%

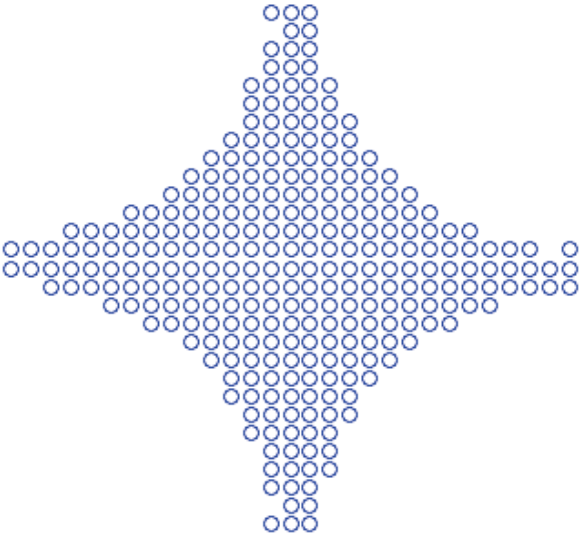

Figure 8: Resulting topology for compliance minimization of square Reissner-Mindlin plates with four edges simply supported and a force loaded at the centre. The material volume fraction is 30%.

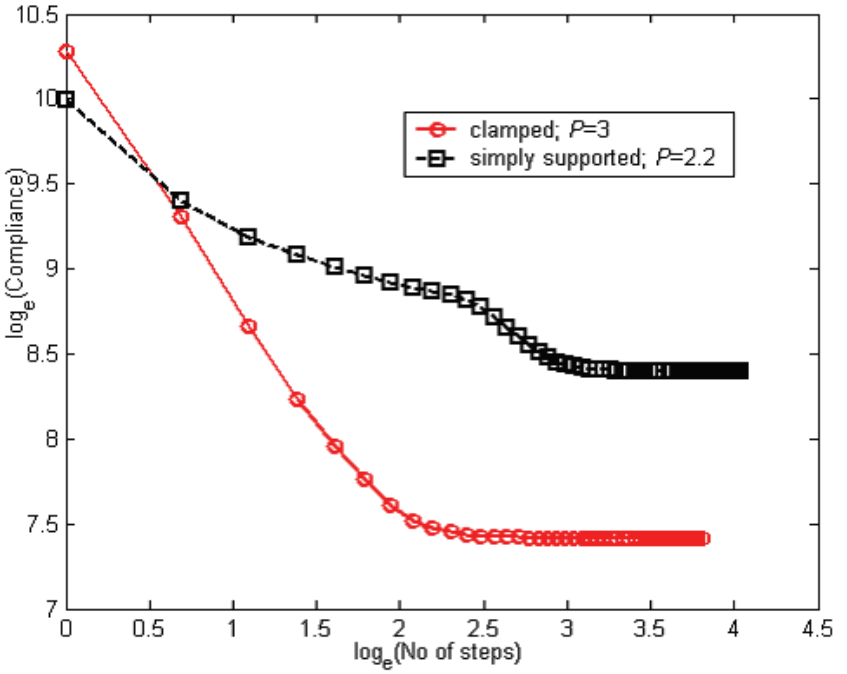

Figure 9: Step-variations of compliance in the optimization process both for the clamped plate and simply supported plate.

References

Atluri S.N; Zhu T. (1998): A new meshless local Petrov–Galerkin (MLPG) approach in computational mechanics. *Computational Mechanics*, vol. 22, pp. 117-127.

Belinha J.; Dinis L.M.J.S. (2006): Elasto-plastic analysis of plates by the element free Galerkin method. *International Journal for Computer-Aided Engineering and Software*. 23 (5): 525-551.

Belytschko T.; Lu Y.; Gu L. (1994): Element free Galerkin methods. *International Journal for Numerical Methods in Engineering*, vol. 37, pp.229-256.

Belytschko T.; Xiao S.P.; Parimi C. (2003): Topology optimization with implicit function and regularization. *Int J Numer Methods Eng*. 57:1177–1196.

Bendsoe M.P. (1989): Optimal shape design as a material distribution problem. *Struct Optim*, 1: 193–202.

Bendsoe M.P.; Kikuchi N. (1988): Generating optimal topologies in optimal de-

sign using a homogenization method. *Comp. Meth. Appl. Mech. Engrg.*, 71: 197–224.

Bendsoe M.P.; Sigmund O. (1999): Material interpolation schemes in topology optimization. *Arch Appl Mech* 69: 635–654.

Bendsoe M.P.; Sigmund O. (2003): *Topology Optimization: Theory, Methods and Applications*. Springer, New York.

Braun J.; Sambridge M. (1995): A numerical method for solving partial differential equations on highly irregular evolving grids. *Nature*, vol. 376, pp. 655-660.

Diaz, A.R.; Lipton, R.; Soto, C.A. (1995): A new formulation of the problem of optimum reinforcement of Ressner-Mindlin plates. *Comput. Methods Appl. Mech. Engrg.* 123(1-4): 121-139.

Donning B.; Liu W.K. (1998): Meshless methods for shear-deformable beams and plates. *Comput Methods Appl Mech Eng.*, 152:47–72.

Fujii D.; Kikuchi N. (2000): Improvement of numerical instabilities in topology optimization using the SLP method. *Struct Multidisc Optim*, 19: 113-121.

Gao L.; Liu K.; Liu Y. (2006): Applications of MLPG Method in Dynamic Fracture Problems, *CMES: Computer Modeling in Engineering& Sciences*, vol. 12, no. 3, pp. 181-196.

Garcia O.A.; Fancello E.A.; Barcellos C.S.; Duarte C.A. (2000): hp-clouds in Mindlin–Reissner thick plate model. *Int J Numer Methods.* 41:1387–1400.

Halkjær, S.; Sigmund O; Jensen J.S. (2006): Maximizing band gaps in plate structures. *Struct Multidisc Optim.* 32: 263–275.

Han Z.D.; Liu H.T.; Rajendran A.M; Atluri S.N. (2006): The Applications of Meshless Local Petrov-Galerkin (MLPG) Approaches in High-Speed Impact, Penetration and Perforation Problems, *CMES: Computer Modeling in Engineering& Sciences*, vol. 14, no. 2, pp. 119-128.

Larsen, A.A.; Laksafoss, B.; Jensen, J.S.; Sigmund, O. (2009): Topological material layout in plates for vibration suppression and wave propagation control. *Struct Multidisc Optim*. 37:585–594.

Lipton, R.; Diaz, A.R. (1997): Reinforced Mindlin plates with extremal stiffness, *International Journal of Solids and Structures*. 24(28): 3691-3704.

Liu W.K; Jun S.; Zhang Y.F. (1995): Reproducing kernel particle methods, *International Journal for Numerical Methods in Fluids*, vol. 20, pp. 1081-1106.

Mindlin R.D. (1951): Influence of rotary inertia and shear on flexural motions of isotropic, elastic plates. *Journal of Applied Mechanics ASME*. 18: 31-38.

Monaghan J.J. (1977): Smoothed particle hydrodynamics: theory and applica-

tions to non-spherical stars, *Monthly Notices of the Astronomical Society*, vol. 181, pp. 375-389.

Pedersen, N.L. (2001): On topology optimization of plates with prestress, *International Journal of Numerical Methods in Engineering*. 51(2): 225-240.

Reissner E. (1945): The effect of transverse shear deformation on the bending of elastic plates. *Journal of Applied Mechanics ASME*. 12: A69-A77.

Sellountos E. J.; Sequeira A.; Polyzos D. (2009): Elastic transient analysis with MLPG(LBIE) method and local RBFs, *CMES: Computer Modeling in Engineering& Sciences*, vol. 41, no. 3, pp. 215-242.

Sladek, J.; Sladek, V.; Krivacek, J.; Wen, P.H.; Zhang Ch. (2007): Meshless local Petrov–Galerkin (MLPG) method for Reissner–Mindlin plates under dynamic load. *Comput. Methods Appl. Mech. Engrg.*, 196: 2681–2691.

Sladek, J.; Sladek, V.; Zhang Ch. (2008a): Local integral equation method for viscoelastic Reissner–Mindlin plates. *Comput Mech.* 41:759–768.

Sladek, J.; Sladek, V.; Solek, P.; Wen, P.H.; Atluri, S.N. (2008b): Thermal Analysis of Reissner-Mindlin Shallow Shells with FGM Properties by the MLPG. *CMES: Computer Modeling in Engineering and Sciences*. 30(2): 77-97.

Soto,C.A.; Diaz, A.R. (1993): On modelling of ribbed plates for shape optimization, *structural Optimization*. 6:175-188.

Svanberg K. (1987): The method of moving asymptotes – a new method for structural optimization. *Int. J. Numer. Meth. Engrg.* 24: 359–373.

Sigmund O. (2001): A 99 line topology optimization code written in Matlab. *Struct. Multidisc. Optim.*, 21: 120–127.

Sigmund O.; Petersson J. (1998): Numerical instabilities in topology optimization: a survey on procedures dealing with checkerboards, mesh-dependencies and local minima. *Struct. Optim.* 16, 68–75.

Sukumar, N.; Moran, B.; Belytschko T. (1998): The natural element method in solid mechanics, *International Journal for Numerical Methods in Engineering*, vol. 43, pp. 839-887.

Wang K.; Zhou S.J.; Shan G.J. (2005): The natural neighbour Petrov-Galerkin method for elasto-statics, *International Journal for Numerical Methods in Engineering*, vol. 63, pp. 1126-1145.

Wang M.Y.; Wang X.; Guo D. (2003): A level-set method for structural topology optimization. *Comp. Meth. Appl. Mech. Engrg.*, 192:227–240.

Wen P.H.; Hon Y.C. (2007): Geometrically Nonlinear Analysis of Reissner-Mindlin Plate by Meshless Computation. *CMES: Computer Modeling in Engineering and*

Sciences. 21(3): 177-191.

Xie Y.M.; Steven G.P. (1993): A simple evolutionary procedure for structural optimization. *Comput Struct*, 49:885–896.

Zhou M.; Rozvany G.I.N. (1991): The COC algorithm, part II: Topological, geometry and generalized shape optimization. *Comp. Meth. Appl. Mech. Engrg.*, 89: 197–224.